Synthetic Method Dependent Physicochemical Properties and Electrochemical Performance of Ni-Doped ZnO

A Chandrasekaran, Thibeorchews Prasankumar, Sujin P Jose, Kandasamy Anitha, Craig Ekstrum, Joshua Pearce, Jeyanthinath Mayandi, Chandrasekaran Abinaya

A. Chandrasekaran, T. Prasankumar, Sujin P Jose, K. Anitha, C. Ekstrum, J. M. Pearce, J. Mayandi. "Synthetic method dependent physico-chemical properties and electrochemical performance of Ni doped ZnO", *Chemistry Select* 2(28), 2017, pp. 9014–9023. doi: https://doi.org/10.1002/slct.201701584

Synthetic method dependent physico-chemical properties and electrochemical performance of Ni doped ZnO

A. Chandrasekaran, [a], T. Prasankumar[b], Sujin P Jose[b, c], K. Anitha[d], C. Ekstrum[e], J. M. Pearce[e, f], J. Mayandi*[a, e]

[a] Department of Materials Science, School of Chemistry, Madurai Kamaraj University, Madurai- 625 021, Tamil Nadu, India.
[b] Department of Computational Physics, School of Physics, Madurai Kamaraj University, Madurai - 625 021, Tamil Nadu, India.
[c] Department of Materials Science and Nano Engineering, Rice University, Houston- 77005, Texas, USA.
[d] Department of Physics, School of Physics, Madurai Kamaraj University, Madurai - 625 021, Tamil Nadu, India.
[e] Department of Materials Science and Engineering, Michigan Technological University, Houghton - 49931, Michigan, USA.
[f] Department of Electrical & Computer Engineering, Michigan Technological University, Houghton - 49931, Michigan, USA.

Abstract

Nickel doped zinc oxide (Ni/ZnO) nanostructures have the potential to improve the performance of electrochemical capacitors. This study investigates the preparation of Ni/ZnO nanomaterials by facile co-precipitation (CPM) and hydrothermal (HTM) methods. The effect of the synthesis methods on the optical, structural, chemical and morphological properties on ZnO products is investigated using ultra violet (UV)-visible spectroscopy, X-ray diffraction (XRD), field emission scanning electron microscopy (FESEM), X-ray spectrometry (EDX), room temperature photoluminescence (PL), Fourier transform infrared (FTIR) and Raman spectroscopy. Finally, the electrochemical performance of the synthesized nanorods were examined by fabrication of a supercapacitor using standard three electrode cell configuration and tested with a cyclic voltammogram (CV) and galvanostatic charge-discharge (GCD) measurements. The results shown that the samples synthesized by HTM exhibited improved electrochemical capacitance performance with higher current density. The discharge curves are linear in the total range of potential with constant slopes, showing perfect capacitance. In conclusion, Ni/ZnO nanoparticles synthesized by this method with further optimization have the potential to lead to a high-efficiency supercapacitors.

Keywords: zinc oxide, Ni doped ZnO, co precipitation method, hydrothermal synthesis, electro-chemical performance

1. Introduction

Zinc oxide (ZnO) nanostructures have drawn significant scientific interest because of its characteristic features and novel application in various fields **[1-7]**. ZnO is a contender for the next generation devices because of its unique opto-electronic properties that include a large band gap (~3.3eV at room temperature), higher values of breakdown voltages (higher than Carbon nanotubes)**[8]**, sustaining large electric fields, high quantum efficiency, higher exciton energy, high-temperature and high-power operations **[9,10]**. ZnO seems to have the richest varieties of nanostructures such as wires **[11]**, tubes **[12]**, rods **[13]**, belts **[14]**, rings **[15]**, springs **[16],** combs **[17]**, flowers **[18]**, and peanuts shapes **[19]**. Numerous methods have been reported for the preparation of nanostructures including precipitative methods (usually aqueous and at low temperature) **[20, 21]**, reactive methods in high boiling point solvents **[22]**, hydrothermal and solvothermal methods **[23]**, and vapour phase reactions **[24]**. Among them co-precipitation (CPM) and hydrothermal (HTM) method have been acknowledged as an effective route for the synthesis of nanostructures for the reason that they are simple, non-hazardous, high yielding and economic. In CPM synthesis a solute that remain dissolved in a solution precipitates out on a carrier that forces it to bind together, rather than remaining dispersed **[25].** It includes three mechanisms such as inclusion, occlusion, and adsorption. In contrast, hydrothermal synthesis is a precise method for crystallizing

substances from high-temperature aqueous solutions at high vapour pressures. A large number of oxide nanoparticles have been synthesized under hydrothermal conditions **[26].** The foremost three mechanisms are hydrolysis, oxidation and thermolysis **[27]**.

Due to the presence of intrinsic defects such as oxygen vacancies (V), zinc vacancies (V_{Zn}) and zinc interstials (Z_{in}) the inherent properties of ZnO do not meet the preferred standard for industrial applications. The ZnO properties can be improved by doping with selected elements. The transition metal doping in semiconductor ZnO facilitates the generation of carrier mediated ferromagnetism **[28].** In specific, nickel is considered to be the most capable transition metal dopant due to its high chemical stability and exceptional ability to tune electrical, optical and magnetic behaviour of ZnO nanostructures [**29]**. Electrochemical capacitors, which have recently received great attention due to their higher power density and higher specific energy than conventional batteries and capacitors **[30]**. In general, carbon materials, metal oxides and conducting polymers are used as electrodes and among the transition metal oxides ruthenium oxide has the highest efficiency **[31]** but due to its cost it has not been commercialized. In order to replace the expensive electrodes, nickel oxide, zinc oxide, manganese oxide and cobalt oxide are widely used because of their pseudo-capacitive behaviour **[32]**. Also the dopants such as Ni, Co Mn in ZnO were extensively studied for various applications such as magnetic, antibacterial, sensors etc., synthesized with simple chemical methods [33-36]. Recently, ZnO with composites such as ZnS, Ni [New ref 1] and some transition metals Al, Co [New ref 2], Fe [New ref 3], Mn [New ref 4] have attained high specific capacity, cycle durability, stable reversible capacity and high lithium storage capacities [New ref 4]. Although ZnO exhibits superior physical properties as battery active material with higher energy density and high efficiency, a very few work has been reported in supercapacitor applications **[33]**. The main cause for this problem is the formation of dendrites during consecutive cycles which lead to the decrease in cycle life **[34]**. Because of its good electrochemical and eco-friendly nature the reported work investigates merging the properties of Ni and ZnO by doping. Quite a few methods have been reported for the synthesis of rod shaped Ni doped ZnO [**35, 36]**.

This work is focused on the preparation of Ni/ZnO nanomaterials by facile co-precipitation and hydrothermal synthesis. The effect of the synthesis routes on the optical, structural, chemical and morphological properties on ZnO is quantified. The electrochemical performance of the synthesized nanorods were examined by the fabricated supercapacitor electrodes using a standard three electrode cell configuration.

2. Experimental Procedure

2.1 Materials

Zinc acetate dihydrate, sodium hydroxide, nickel (II) nitrate hexahydrate were purchased from Merck with 98%, 97% and 97% purity, respectively. Distilled water was used as the solvent and all the chemicals were used without further refining.

2.2 Characterization Techniques

The crystal structure of the ZnO nanocrystals was determined by a Bruker X-ray diffractometer (Model AXS D8 Advance using Cu Wavelength 0.1546 nm). The morphological features were recorded by Hitachi S-4700 FESEM and an elemental composition was obtained using an FEI Philips XL energy-dispersive X-ray spectrometer. The optical absorption and emission spectra of ZnO dispersed in distilled water were recorded using Agilent 8453 UV-Visible spectrophotometer and Agilent spectrofluorometer carry eclipse. The FT-IR spectra of the sample were obtained with a Thermo Nicolet 6700 and Raman scattering measurements were performed using Horiba Jobin Yvon Lab Ram HR800 equipped with a CCD detector. All the electrochemical measurements were carried out using Bio-Logic (SP-50) electrochemical workstation.

2.3 Synthesis by Co-Precipitation Method

Initially, 3 g of zinc acetate dihydrate and 5 wt % of nickel (II) nitrate hexahydrate was dissolved in 75 ml of double distilled water and kept stirring for 15 m. Sodium hydroxide solution

had been prepared separately by dissolving 2.4 g of NaOH in 75 ml of double distilled water. The prepared NaOH solution was added drop-wise into the initial precursor solution under constant stirring at room temperature. The mixed solution was kept under stirring for 30 m. The gelatinous precipitates was then kept on the hot plate at a temperature of 80ºC for 5 h. After that the solution was washed with distilled water and ethanol for several times using a centrifuge. The final precipitate was collected and dried at 120ºC by means of hot plate for 1 h in atmosphere.

2.4 Synthesis by Hydrothermal Method

In this method, 3 g of zinc acetate dihydrate was dissolved in 75 ml of double distilled water with 5wt % of Ni $(NO_3)_2.6H_2O$. The buffer solution was prepared by taking 2.4 g of NaOH in 75 ml of distilled water. This solution was added drop by drop to the Ni doped Zn solution under stirring. The initial solution containing milky coloured precipitate was kept for stirred for 30 m. The resulting solution was kept in an autoclave and placed inside a muffle furnace at a temperature of 160ºC for 5 h. The obtained precipitate was then washed with distilled water and ethanol 3 times respectively and dried at 120ºC for 1 h using hot plate.

2.5 Fabrication of electrode

The working electrode was prepared by mixing of 80 wt% of Ni/ZnO as active material, 15 wt% of acetylene black as conducting agent and 5 wt% of PVDF (polyvinylidene fluoride) as binder with few drops of n-methylpyrrolidone (NMP) as solvent. The prepared slurry was pasted onto a pre cleaned carbon felt. The substrate was dried at 100°C for 12 hrs which was then employed as working electrode.

2.6 Electrochemical Tests

Supercapacitor behaviour of the Ni/ZnO nanoparticles was studied using CV and GCD measurements. The electrochemical properties of the samples were carried out using three electrode cell configurations with Ni/ZnO electrode as the working electrode, Ag/AgCl as the reference electrode while a platinum wire as the counter electrode. 1 M KOH aqueous solution was used as the electrolyte.

3. Result and Discussion

3.1 XRD

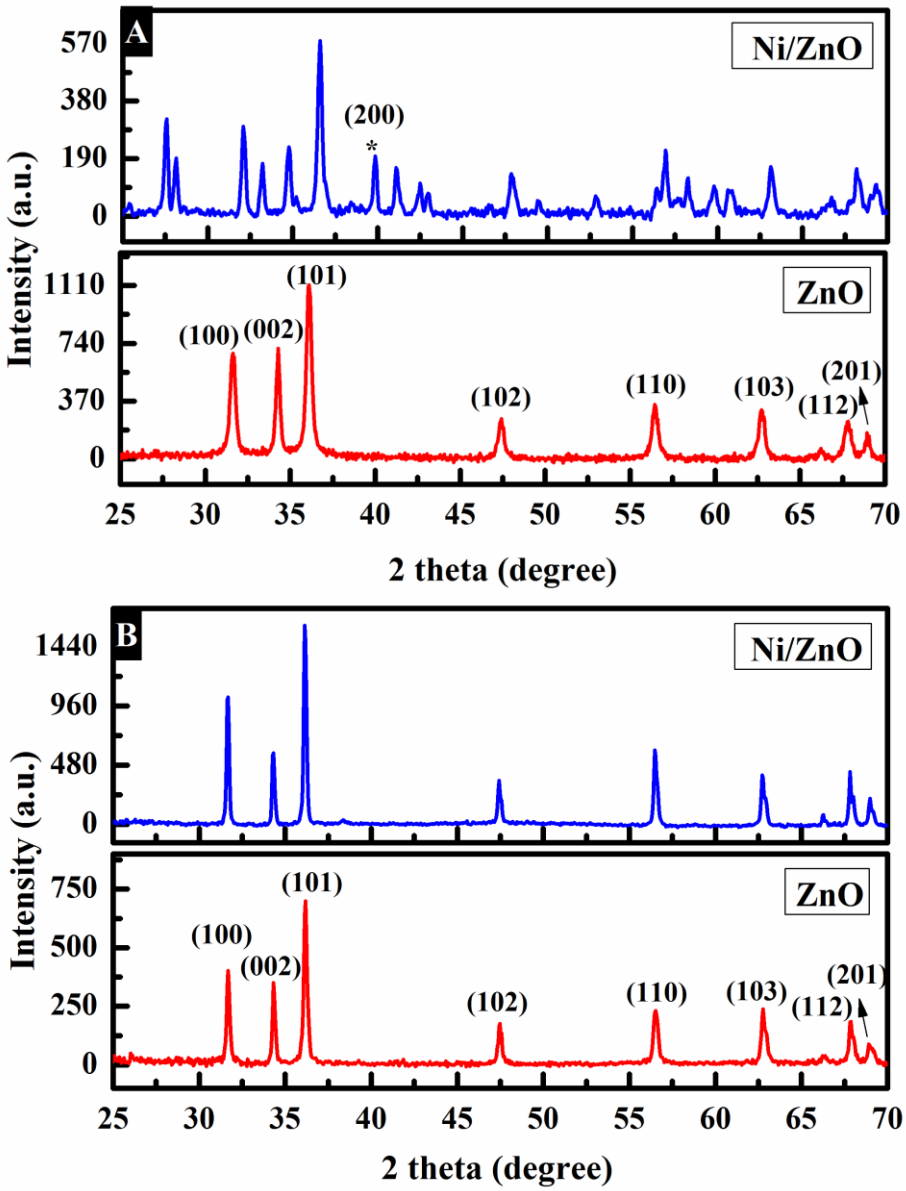

Figure 1 Powder diffraction pattern of pure and Ni/ZnO nanoparticles synthesized by CPM (A) and HTM (B) (*indicates the presence of Ni).

Figure 1 (A) and (B) depicts the XRD pattern of pure and Ni doped ZnO nanoparticles prepared by co-precipitation and hydrothermal method in the range from 25º to 70º. The peaks observed in the XRD pattern confirm the polycrystalline nature of the nanoparticle, with (100), (002), (101), (102), (110), (103), (112) and (201) reflections of pure ZnO phase with the hexagonal wurtzite structure (JCPDS card No. 89-0510). Altogether the reflections were highly oriented along the most stable phase (101) of ZnO and it is used for further calculations. In Figure 1 (A) an additional peak at 43.29 º was observed and it can be indexed for the (200) reflection of nickel oxide (NiO). It shows that the Ni/ ZnO was formed along with the NiO phase and its noteworthy this secondary phase was exhibited only by the nickel doped ZnO prepared by CPM. El-hilo et al., have reported that 4.3% of Ni doped ZnO nano-particles exhibited NiO phases **[37]**. The additional peaks observed in the Ni/ZnO by CPM were attributed to the presence of zinc hydroxide (JCPDS card No. 01-0360). Diffraction peaks corresponding to NiO or impurities were not observed in the XRD patterns of

HTM, confirming the high purity of synthesized product **[38]**. Table 1 shows the average crystallite sizes of the samples calculated by Debye Scherrer's equation (equation 1)

$$D = (0.9\lambda)/(\beta \cos \theta) \text{ ---------- (1)}$$

Where, D is the diameter of the crystallite, λ is the wavelength of Cu Kα line (1.5406 Å), β is the full width at half maximum (FWHM) in radians and θ is the Bragg angle.

Parameters		ZnO		Ni /ZnO	
		CPM	HTM	CPM	HTM
D Spacing(Å)		2.488	2.481	2.455	2.483
Lattice Constants (Å)	a	3.270	3.259	3.254	3.262
	c	5.328	5.266	5.236	5.282
Bond Length L (Å)		2.00	1.98	1.98	1.99
Grain Size (nm)	101 Plane	24	38	30	49
	Average	25	36	39	47
Dislocation Density $10^{-3}(nm^{-2})$		1.585	0.778	0.719	0.524
Micro Strain		0.0014	0.0009	0.0011	0.0007
Volume of unit cell $(Å)^3$		49.368	48.609	45.044	48.690
Net Lattice Distortion		0.0052	0.0026	-0.0081	0.0032

Table 1. XRD parameters of the pure and Ni/ZnO samples by CPM and HTM

The larger size (47 nm) was observed for the Ni doped ZnO nanoparticles synthesized by HTM. Table 2 shows the particle size and strain of pure and Ni doped ZnO. Compared to the co-precipitation method, the hydrothermally synthesized samples exhibited the highest grain size values. The similar ionic radii 0.74 for $Zn^{2+}$and 0.69Å for Ni^{2+}**[39-41]**,the substitution of Ni^{2+} for Zn^{2+} doesn't result in noticeable lattice distortion and there was no shift observed in the diffraction peaks except for the intensity changes in doped samples.

Sample Name	Particle size (nm)		Strain	
	CPM	HTM	CPM	HTM
Pure ZnO	43	110	0.00109	0.00155
Ni/ZnO	67	112	0.00154	0.00112

Table 2. Particle size and strain of the pure and Ni/ZnO samples by CPM and HTM

3.2 FE-SEM Analysis

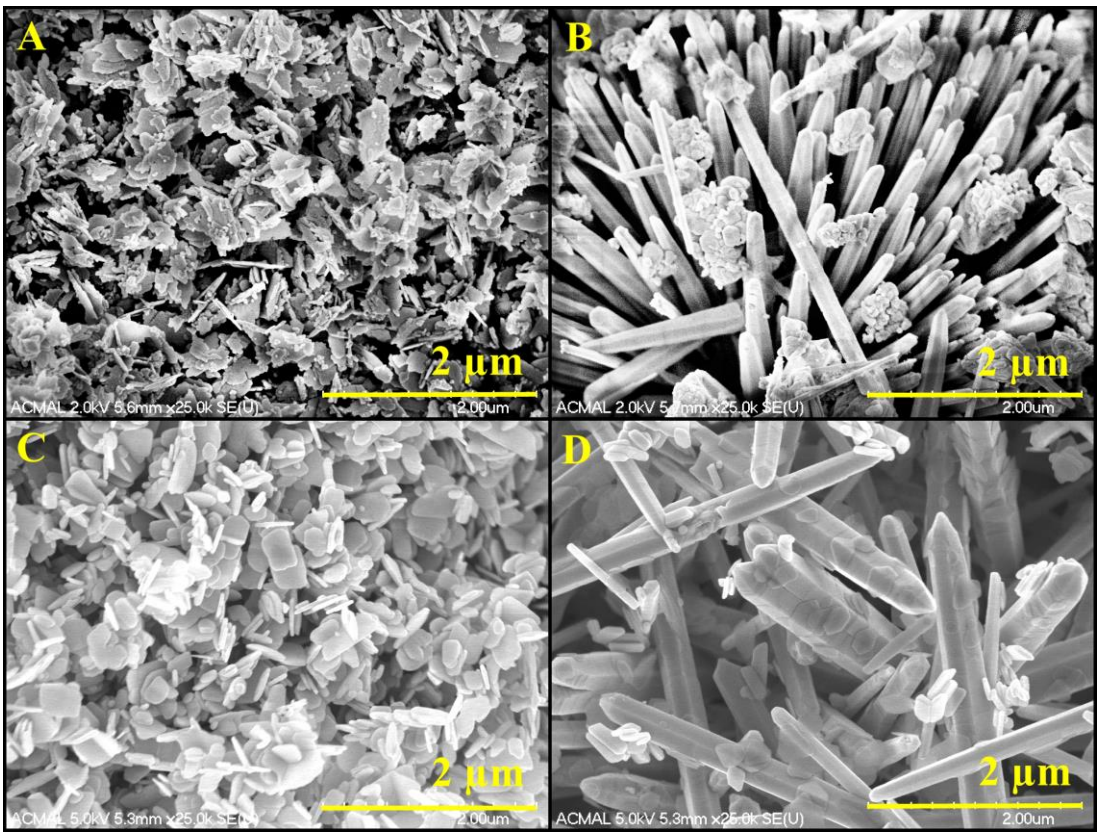

Figure 2 Morphology of pure ZnO by CPM (A), Ni/ZnO by CPM (B), pure ZnO by HTM (C) and Ni/ZnO by HTM (D)

The morphology of the pure and Ni/ZnO synthesized by CPM (A, B) and HTM (C, D) are shown in Figure 2. The pure ZnO's were observed as nanoplates, which were influenced by Ni to form as nanorods, with the absence of any porosity. Both CPM and HTM nanorods were randomly arranged and aligned in small stacks. The pure ZnO and Ni/ZnO (C & D) by HTM shows the respective morphologies as nanoplates and nanorods. These morphologies are similar to those produced through CPM. The nanoplates produced by HTM have smoother edges than those from CPM, and have fewer small platelets attached to their faces. HTM nanorods tend to be thicker than those produced by CPM. Some free nanoplates are present in both the nanorod images (B and D). However, the platelets are distributed differently. Comparing with HTM, samples produced by CPM show densely packed with agglomerated particles, distributed throughout the structure. In HTM samples, the nanoplates tend to be more aligned, their faces being parallel, and are affixed to the flat faces of the nanorods. Noting the shape of the nanoplates between the Ni-doped ZnO and the undoped ZnO, the HTM nanoplates affixed to the nanorods appear to be more hexagonal than the undoped variety. It is clear that Ni influence the formation of nanorods with narrow tipped prismatic hexagonal surfaces. It is interesting to note the horizontal streaks, and steps, perpendicular to the axis of the nanorods. This feature is more apparent in the HTM-nanorods than the CPM-nanorods, which may only be an artefact of image quality. These lamellar lines supports the claim that the nanorods are indeed stacks of nanoplates, and have been influenced to align around an axis. The diameter of the nanorods slightly but gradually decreases towards the end of the tip. It is reasonable to assume that the incorporation of external impurity into the lattice of ZnO without altering the overall structure may cause the formation of rods and agglomeration. Experimental conditions in both the methods affect the morphology and size of growing crystal.

Figure 3 (A & B) shows a representative EDAX pattern and the details of the relevant elemental analysis for Ni/ZnO by CPM (A) and HTM (B).

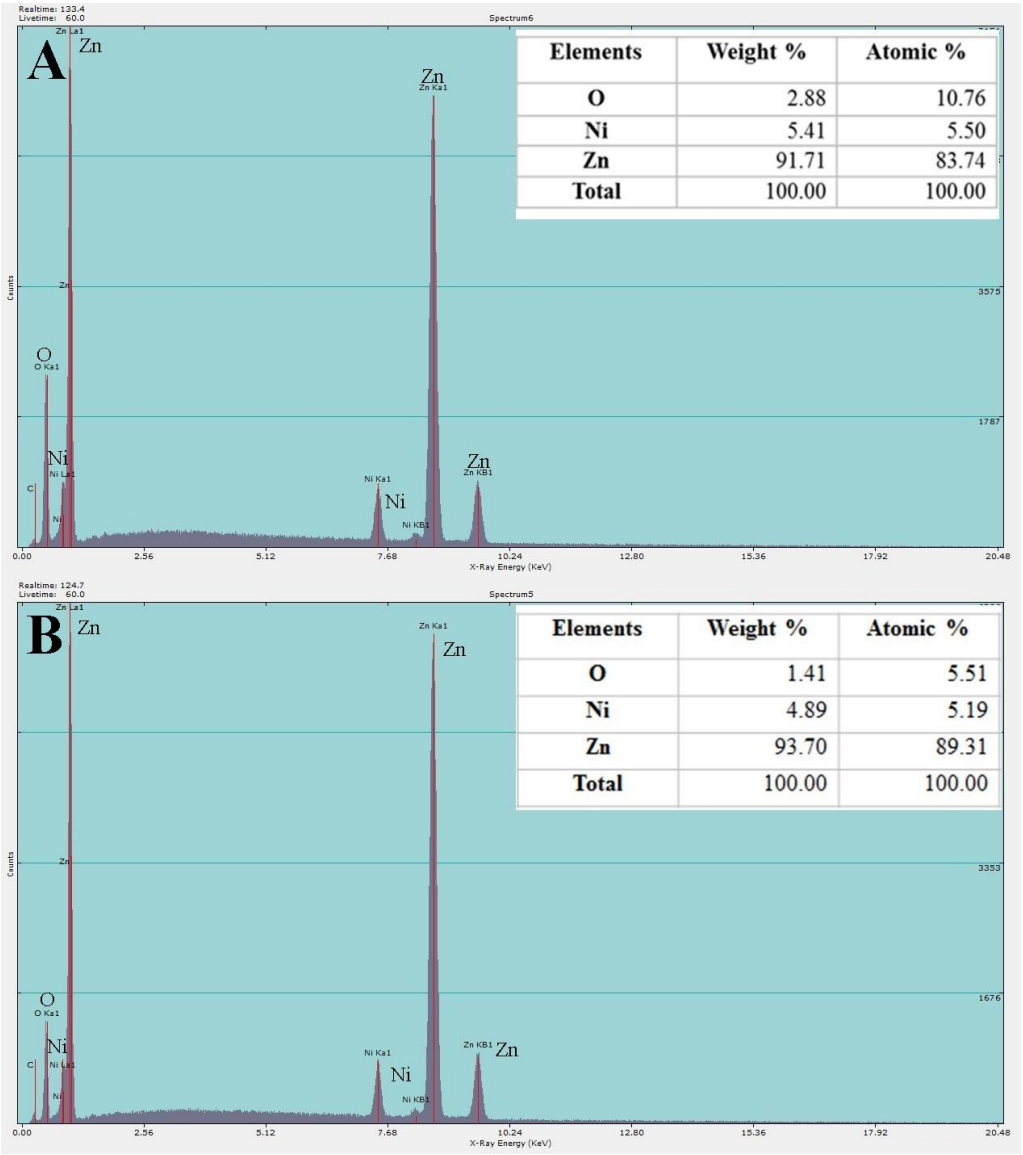

Figure 3 Elemental composition of Ni/ZnO by CPM (A), Ni/ZnO by HTM (B)

The pattern shows strong Zn and O peaks without any impurity confirming the purity of the samples. The presence of Ni confirms that Ni ions were doped into ZnO nanostructures. Also notable is the difference in oxygen content, between the CPM and HTM samples: The CPM sample contains more oxygen. EDAX also measures more Ni content in the CPM sample, at 5.41 wt%, than the HTM sample, which is measured to have 4.89 wt% Ni, which corresponds to heavier doping of the CPM sample.

3.3 UV-Visible Spectral Analysis

The UV-visible absorption spectra of the as-prepared co-precipitation and hydrothermally synthesized pure ZnO and Ni/ZnO with different morphology was examined and shown in Figure 4 (A) and (B).

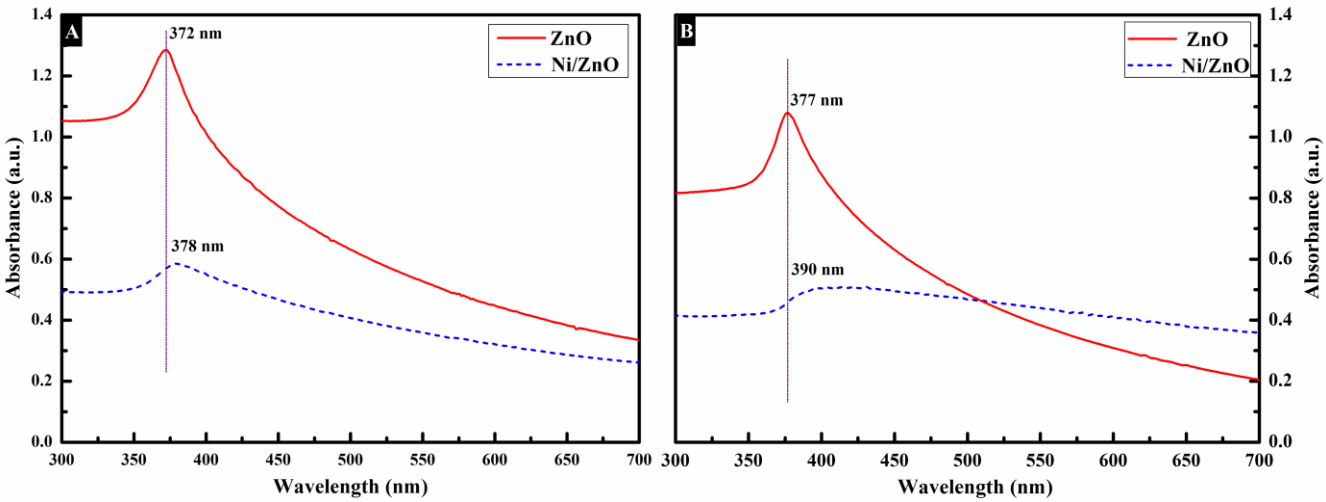

Figure 4 UV spectra of pure and Ni/ZnO synthesized by CPM (A) and HTM (B)

As displayed all the samples exhibit an optical absorption below 400 nm due to the surface state of ZnO **[42]**. The absorption peak appeared at about 372 nm and 377 nm for CPM and HTM ZnO samples, respectively (Table 3). On incorporation of nickel, the absorption peak shifted towards higher wavelength, which resulted in the decrease of bandgap energy. The peak was very broad with a red shift and this can be attributed to the defect states between valence band and conduction band (O_{2p} → Zn_{3d}) **[43]** and higher scattering at the surfaces of nanorods **[44]**. The Ni doping in ZnO causes the slight tapering of bandgap for both the cases.

ZnO is a directband gap semiconductor, and therefore its absorption coefficient is related to the excitation energy

$$\alpha h\upsilon = C\,(h\upsilon - E_g)^{1/2} \qquad (2)$$

where α is the absorption coefficient hυ is the incident photon energy C is the constant and E_g is the direct band gap in eV {(E_{exc}= hν) by $(\alpha h\nu)^2 = C\,(h\nu - E_g)$}. To obtain the absorption onset, $(\alpha h\nu)^2$ was plotted versus energy hν. Extrapolation of the linear part until its intersection with the hν axis gives the values of E_g. By knowing the value of absorbance and wavelength from the data, the optical band gap of ZnO was estimated by Tauc's plot **[45]** and it is shown in table 3:

Sample Name	Absorption edge (nm)		Band gap (eV)	
	CPM	HTM	CPM	HTM
Pure ZnO	372	377	3.34	3.29
Ni/ ZnO	378	390	3.29	3.19

Table 3. Shows the absorption edge and bandgap of pure and Ni/ZnO samples by CPM and HTM

3.4 Photoluminescence

Figure 5 shows the room temperature PL spectra of the pure and Ni/ZnO nanoparticles as-synthesized by CPM (A) and HTM (B).

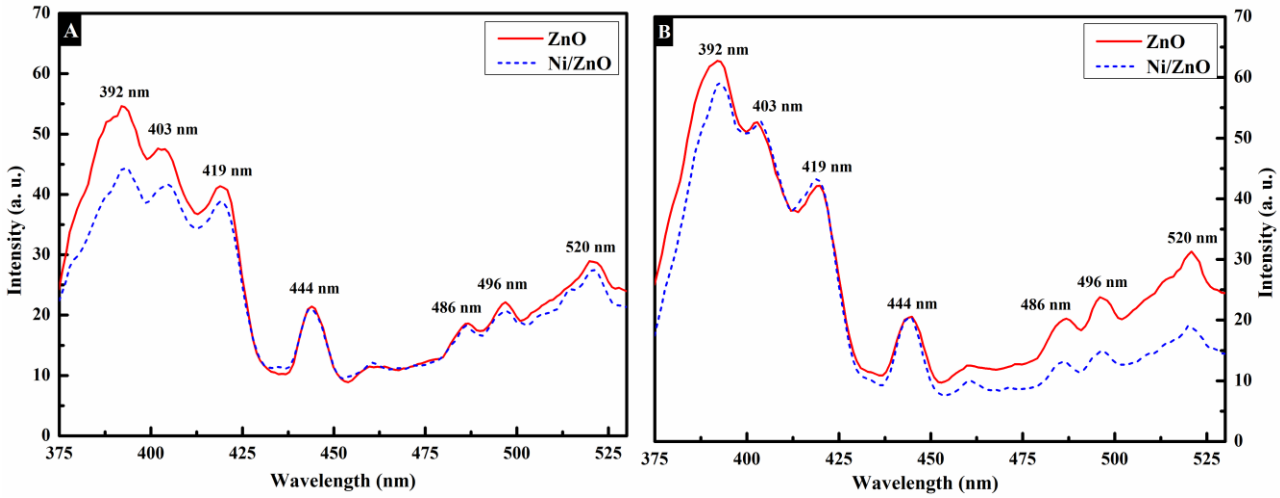

Figure 5 Emission spectra of pure and Ni/ZnO synthesized by CPM (A) and HTM (B)

The PL measurements were performed at an excitation wavelength of 325 nm. Excitonic emissions were observed from the photoluminescence spectra of ZnO nanomaterials. All the samples were optically similar with the emission peaks centered at 392 nm, 403 nm, 419 nm (violet emission), 444 nm (blue emission), 460 nm, 486 nm (blue green emission), 496 nm and 520 nm (green emission) irrespective of the method of preparation. The asymmetric spectra were due to the native defect states of ZnO **[46]**. The strong emission peak at 392 nm may be attributed to near band edge emission **[47]** and the peak at 403 nm was originated due to defect states **[48]**. Many researchers showed that the other visible emissions may be due to the zinc interstitials, zinc vacancies and oxygen vacancies **[49-51]**. The oxygen vacancies were responsible for the green emission at 520 nm **[52]**. The intensity of emission mainly depends on surface states and the luminescence properties depend on the properties of the surface **[53]**. The strong UV and weak visible bands imply good crystal surface **[54]**.

3.5 FTIR

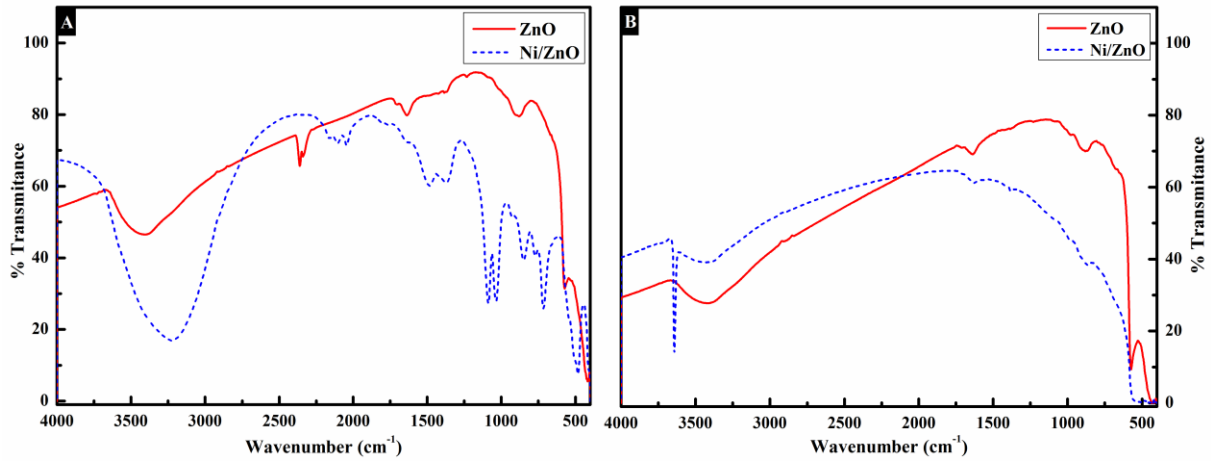

Figure 6 FTIR spectra of pure and Ni/ZnO synthesized by CPM (A) and HTM (B)

Infrared spectroscopy was used to detect the presence of functional groups adsorbed on the surface of synthesized nanoparticle. FTIR spectra of pure ZnO and Ni/ZnO synthesized by CPM and HTM methods are shown in Figure 6 (A & B). In the co-precipitation method the broad absorption band at 3385 cm^{-1} corresponds to the O–H stretching vibration of water present in ZnO **[55]** and the absorption peak at 2358 cm^{-1} is because of an existence of CO_2 molecule present in the atmosphere **[56]**. In the hydrothermal method some slight changes are observed compared to co-precipitation method. The band at 1643 cm^{-1} (CPM) and the band at 1637 cm^{-1} (HTM) can be associated with the H-OH stretching **[57]**. In the CPM method the transmission band at ~1361 cm^{-1} the sample was due to

the asymmetric stretching of acetate species from precursor **[58]** and this band was not observed in hydrothermally synthesized samples. The band appearing at 877 cm^{-1} in both the methods was due to the formation of tetrahedral co-ordination of Zn **[59]**. The peaks appearing between 400 cm^{-1} to 570 cm^{-1} were assigned to the Metal-Oxygen (M-O) stretching mode **[60]**. But in the case of Ni^{2+} more changes in peak intensity were observed. The vibration modes at 720 cm^{-1} & 1086 cm^{-1} in CPM and 1430 cm^{-1} in HTM were associated with Ni^{2+} occupation at Zn^{2+} sites **[61]**. Because of ionic radii mismatch between Ni^{2+} intrinsic host lattice defects are activated. This type of activated impurity causes a shift in the vibration mode **[62]**.

3.6 Raman Spectroscopy

The vibrational modes of ZnO might be changed by dopants, so Raman spectra of pure ZnO by CPM (A), Ni/ZnO by CPM (B), Pure ZnO by HTM (C) and Ni/ZnO by HTM (D) were measured and shown in Figure 7.

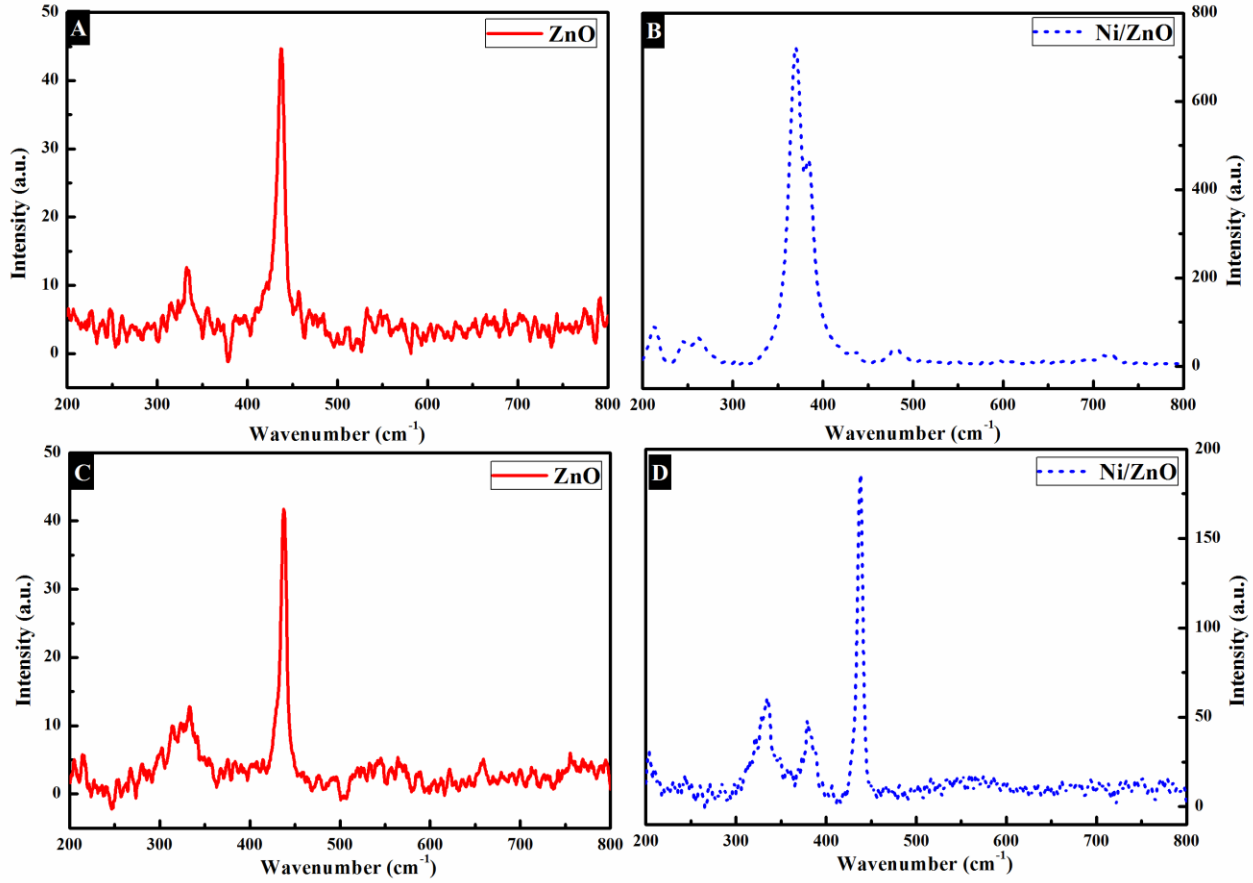

Figure 7 Raman spectra of pure ZnO by CPM (A), Ni/ZnO by CPM (B), Pure ZnO by HTM (C) and Ni/ZnO by HTM (D)

Typically there are two polar branches, one non polar branch and eight sets of optical phonon modes in wurtzite ZnO crystal. The polar branches A_1 and E_1 split into longitudinal (LO) and transverse (TO) optical components with different frequencies. The non polar branch E_2 contains low and high frequency phonons (E_{2L} and E_{2H}) **[63].** In which E_{2L} is associated to the heavy zinc sublattice and E_{2H} associated only with oxygen atoms **[64]**. The phonon modes near the center of the Brillion zone (G point) may be written as: $\Gamma=A_1+2B_1+E_1+2E_2$. Among these modes, A_1, E_1 and $2E_2$ are Raman active and $2B_1$ is Raman inactive or forbidden mode for ZnO **[65].** It is observed that the peak at 331cm^{-1} and an intense peak at 438 cm^{-1} were consistent with A_1(TO) and E_2(high) vibration modes. For Ni/ZnO, an peak at 372 cm^{-1} (CPM) and 379 cm^{-1} (HTM) was observed and assigned to E_2(high)-E_2(low) modes **[66]**. It can be seen that there was a blue shift with additional peaks located for the Ni/ZnO by CPM due to the lattice-host intrinsic defect. The breakdown of translational crystal

symmetry in the samples produced by co precipitation method was because of the incorporated defects and impurities. This indicates that that the ZnO was damaged, but still retains its wurtzite lattice structure.

3.7 Electrochemical Characterizations

Cyclic Voltammetry

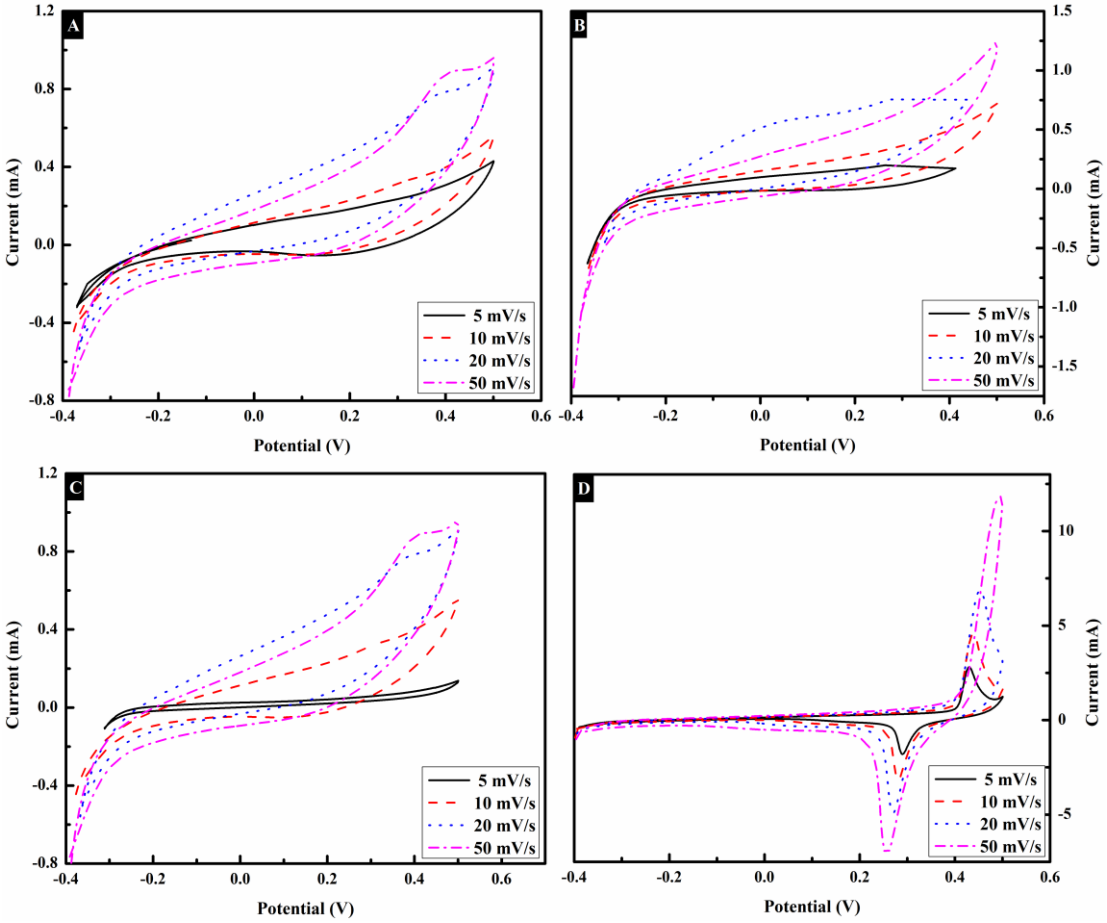

Figure 8.Cyclic Voltammograms of pure ZnO by CPM (A), Ni/ZnO by CPM (B), Pure ZnO by HTM (C) and Ni/ZnO by HTM (D) at scan rates 5, 10, 20 and 50 mV/s.

Figure 8 shows the cyclic voltammograms of bare and Ni/ZnO electrodes by CPM (A, B) and HTM (C, D) in 1 M KOH recorded at the scan rates of 5, 10, 20, and 50 mV/s. The cyclic voltammetry of the electrode materials were performed between the potential windows of -0.4V to 0.5V. All the samples exhibit quasi-rectangular ~~like~~ shape, reversible and capacitive behaviour. By changing the scan rate, the power properties of the electrodes were evaluated and the results are shown in Figure 8. It can be seen from the CV curves that the scan rate and the current response were directly proportional. For the pure and Ni/ZnO by CPM and HTM it was observed that the Ni/ZnO has better capacitive current. The Ni/ZnO electrode by HTM shows a pair of Faradaic redox peaks with high capacitive current (~12 mA) comparing all other electrodes. These redox peaks were formed due to the intercalation and de-intercalation of K^+ ions from the electrolyte into ZnO. The energy storage in these electrodes is due the accumulation of ionic charge in the double layer at the electrode/electrolyte interface. This implies that, of all the samples Ni/ZnO (HTM) electrode has good capacitive performance which may be due to pseudo-capacitance of the electrochemically active ZnO nanorods, fast reversible redox reaction and effective electrical and ionic conductivity of Ni^{2+} and Zn^{2+}.

Galvanostatic Charge Discharge of Ni/ZnO Electrodes

The charge-discharge measurements for bare and Ni/ZnO electrodes by CPM (A, B) and HTM (C, D) were carried out using chronopotentiometry at different current densities in the potential window of -0.4V to 0.5V and the corresponding results were shown in Figure 9.

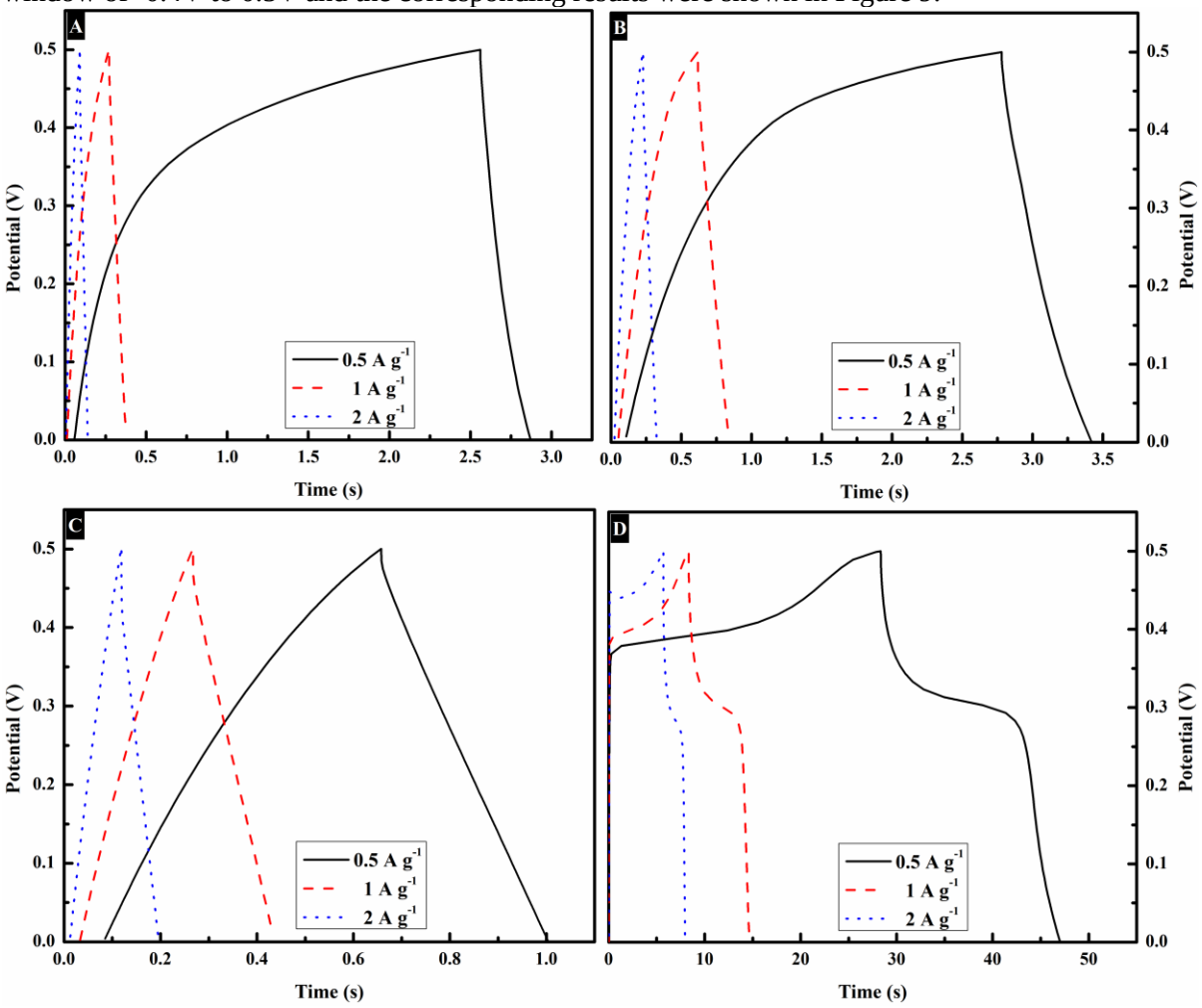

Figure 9 Galvanostatic charge–discharge curves of pure ZnO by CPM (A), Ni/ZnO by CPM (B), Pure ZnO by HTM (C) and Ni/ZnO by HTM (D) hybrid electrode at different current densities.

The charge–discharge properties of ZnO electrodes in 1 M KOH were investigated with different current densities of 0.5, 1 and 2 A g^{-1}. The charge and discharge curves exhibit excellent reversibility for forward and backward reaction processes. A pseudo-capacitance behaviour of ZnO was observed for pure and Ni/ZnO by CPM. Meanwhile, it should be noted that the curves for pure ZnO by HTM shows a nearly linear relationship, which is an ideal capacitive behaviour. The voltage decreases linearly with the increase of discharge time. A nonlinear double-layered discharge curve was obtained for Ni/ZnO by HTM with increased capacitance. This may be due to defect rich nickel and zinc oxide and electrochemical adsorption–desorption or redox reaction at the electrode and electrolyte interface. The average specific capacitance of the electrodes can be calculated using the formula (equation 3):

$$C_m = It/\Delta V_m \text{ ---------- (3)}$$

where, C_m, I, t and ΔV are the specific capacitance of electrodes (F g^{-1}), the charge-discharge current (A), the discharge time (s) and the mass of electrode, respectively.

Due to the incorporation of Ni as extrinsic impurity into the zinc oxide matrix, enormous oxygen vacancies were generated which leads empty oxygen sites. Thus the interstitial occurrence of zinc and Ni ions will promotes the ionic conductivity. This may leads to have either shallow or deep level donors in the bandgap of ZnO . In the present investigation the results show that the preparation condition of the composite electrodes by the hydrothermal method helps in getting high defect

content of zinc oxide with nickel, in increasing charge carriers, and enhancing double layer capacitance.

4. Conclusions

This study compares two different types of synthesis of Ni/ZnO using the co-precipitation and hydrothermal methods. CPM provides an inexpensive route to the synthesis of many nanoparticle materials, but it lacks the reaction control needed for high quality crystallinity and purity of the materials. These challenges were overcome with the use of the hydrothermal method. In the UV optical analysis the HTM samples were slightly shifted towards the visible region when compared to CPM samples, which is due to the generation of more absorption states or defect energy bands. In the emission, both the samples have similar defect peaks with only change in intensity. In FTIR analysis it is observed that the transmission band for the carbonyl group of the carboxylate ions was absent in HTM samples, which shows that the precursor peaks were removed by the hydrothermal condition. Raman analysis also showed that the HTM samples have defect free crystallinity. The CV curve suggests that the electrochemical capacitance performances of the Ni/ZnO by HTM are good with highest current density than by CPM. The discharge curves are linear in the total range of potential with constant slopes, showing perfect capacitive behaviour for Ni doped sample prepared by hydrothermal synthesis. In conclusion, the electrodes fabricated using HTM shows good efficiency when compared to the samples prepared with the co-precipitation method. These preliminary findings open up new opportunities for Ni/ZnO nanoparticles in applications of electrochemical supercapacitors as well as other energy storage devices. Ni/ZnO nanoparticles synthesized by this method with further optimization have the potential to lead to a high-efficiency supercapacitors.

Acknowledgement

AC thanks the DST-INSPIRE New Delhi, India for the financial assistance as fellowship. JM, thanks the DST-SERB for the partial support through the project SERB/F/1829/2012-13. JM and SPJ thank UGC, New Delhi, INDIA for providing support through RAMAN fellowship (2014-2015). SPJ, wishes to acknowledge UGC-MRP programme for providing financial support through the project F.No. 42-793/2013 (SR). CE and JMP thank the MacArthur Fellowship for support.

References

1. E. Kaidashev, M. Lorenz, H. Von Wenckstern, A. Rahm, H.C.Semmelhack, K. H. Han, G. Benndorf, C. Bundesmann, H. Hochmuth, M. Grundmann, High electron mobility of epitaxial ZnO thin films on c-plane sapphire grown by multi step pulsed-laser deposition, Appl. Phys. Lett., 82 (2003) 3901-3903.
2. F. Pirot, J. Millet, Y.N. Kalia, P. Humbert, In vitro study of percutaneous absorption, cutaneous bioavailability and bioequivalence of zinc and copper from five topical formulations, Skin Pharmacol., 9 (1996) 259-269.
3. Z.H. Lim, Z.X. Chia, M. Kevin, A.S.W. Wong, G.W. Ho, A facile approach towards ZnO nanorods conductive textile for room temperature multifunctional sensors, Sens. Actuators B Chem. , 151 (2010) 121-126.
4. M. Purica, E. Budianu, E. Rusu, ZnO thin film on semiconductors materials substrate for large area photo-detector applications, Thin Solid Films, 383 (2001) 284-286.
5. S.H. Jo, J.Y. Lao, Z.F. Ren, R.A. Farrer, T. Baldacchini, J.T. Fourkas, Field-emission studies on thin films of zinc oxide nanowires, Appl. Phys. Lett., 83 (2003) 4821-4823.
6. F.C. Lin, Y. Takao, Y. Shimizu, M. Egashira, Hydrogen-Sensing mechanism of Zinc-oxide varistor gas sensors, Sens. Actuators B Chem., 24 (1995) 843-850.
7. M. Wang, X. Wang, Electrodeposition zinc-oxide inverse opal and its application in hybrid photovoltaics, Sol. Energy Mater. Sol. Cells, 92 (2008) 357-362.
8. L. Liao, H.B. Lu, M. Shuai, J.C. Li, Y.L. Liu, C. Liu, Z.X. Shen and T. Yu, A novel gas sensor based on field ionization from ZnO nanowires: moderate working voltage and high stability, Nanotechnology, 19 (2008) 175501-175506.
9. M. Li, H. Bala, X. Lv, X. Ma, F. Sun, L. Tang, Z. Wang, Direct synthesis of monodispersed ZnO nanoparticles in an aqueous solution, Mater. Lett., 61 (2007) 690-693.

10. V. Cracium, J. Elders, JGE. Gardeniers, J. Geretovsky, Ian W. Boyd, Growth of ZnO thin films on GaAs by pulsed laser deposition. Thin Solid Films, 259 (1995) 1-4.
11. M.H. Huang, Y. Wu, H. Feick, N. Tran, E. Weber, P. Yang, Catalytic growth of zinc oxide nanowires by vapor transport, Adv. Mater., 13 (2001) 113-116.
12. H. Yu, Z. Zhang, M. Han, X. Hao, F. Zhu, A general low-temperature route for large-scale fabrication of highly oriented ZnO nanorod/nanotube arrays, J. Am. Chem. Soc., 127 (2005) 2378-2379.
13. I. Gonzalez-Valls, Y. Yu, B. Ballesteros, J. Oro, M. Lira-Cantu, Synthesis conditions, light intensity and temperature effect on the performance of ZnO nanorods-based dye sensitized solar cells, J. Power Sources, 196 (2011) 6609-6621.
14. Z.W. Pan, Z.R. Dai, Z.L. Wang, Nanobelts of semiconducting oxides, Science, 291 (2001) 1947-1956.
15. X.Y. Kong, Y. Ding, R.S. Yang, Z.L. Wang, Single-crystal nanorings formed by epitaxial self-coiling of polar nanobelts, Science, 303 (2004) 1348-1351.
16. X.Y. Kong, Z.L. Wang, Spontaneous polarization-induced nanohelixes, nanosprings, and nanorings of piezoelectric nanobelts, Nano Lett., 3 (2003) 1625-1631.
17. Z.L. Wang, X.Y. Kong, J.M. Zuo, Induced growth of asymmetric nanocantilever arrays on polar surfaces, Phys. Rev. Lett., 91 (2003) 185502-185506.
18. Parasharam M. Shirage, ZnO nano-flowers, Materials Today, 16 (2013) 505-506.
19. M. Prabhu, J. Mayandi, R.N. Mariammal, V. Vishnukanthan, J.M. Pearce, , N. Soundararajan, K. Ramachandran, Peanut shaped ZnO microstructures: controlled synthesis and nucleation growth toward low-cost dye sensitized solar cells, Materials Research Express, 2 (2015) 066202-066208.
20. C. Chen, P. Liu, C. Lu, ZnO nano-flowers, Chem. Eng. J., 144 (2008) 509-513.
21. O.D. Jayakumar, H.G. Salunke, R.M. Kadam, M. Mohapatra, G. Yashwant, S.K. Kulshreshtha, Magnetism in Mn-doped ZnO nanoparticles prepared by a co-precipitation method, Nanotechnology, 17 (2006) 1278-1285.
22. Th. Agne, Z. Guan, X.M. Li, H. Wolf, Th. Wichert, H. Natter, R. Hempelmann, Doping of the nanocrystalline semiconductor zinc oxide with the donor indium, Appl. Phys. Lett., 83 (2003) 1204-1207.
23. S. Ameen, M.S. Akhtar, H.K. Seo, Y.S. Kim, H.S. Shin, Influence of Sn doping on ZnO nanostructures from nanoparticles to spindle shape and their photoelectrochemical properties for dye sensitized solar cells, Chem. Eng. J., 187 (2012) 351-356.
24. C.X. Xu, X.W. Sun, B.J.P. Chen, Field emission from gallium-doped zinc oxide nanofiber array, Appl. Phys. Lett., 84 (2004) 1540-1542.
25. Harvey, D., Modern Analytical Chemistry. McGraw-Hill, United States of America, 2000
26. C. N. R. Rao, A. Miller, A. K. Cheetham, The chemistry of Nanomaterials: Synthesis, Properties and Applications, Wiley- VCH Verlag GmbH & Co. KGaA, 2004.
27. M. Rajamathi, R. Seshadri, Oxide and chalcogenide nanoparticles from hydrothermal/solvothermal reactions, Curr. Opin. Solid State Mater. Sci., 6 (2002) 337-345
28. S.J. Pearton, C.R. Abernathy, M.E. Overberg, G.T. Thaler, D.P. Norton, N. Theodoropoulou, A. F. Hebard, Y. D. Park, F. Ren, J. Kim, L. A. Boatner, Wide band gap ferromagnetic semiconductors and oxides. J. Appl. Phys., 93 (2003) 1-13.
29. F. Ahmed, N. Arshi, M.S. Anwar, S.H. Lee, E.S. Byon, N.J. Lyu, B.H. Koo, Effect of Ni substitution on structural, morphological and magnetic properties of Zn1−xNixO nanorods, Curr. Appl. Phys., 12 (2012) 174-177.
30. J. Bae, M. K. Song, Y. J. Park, J. M. Kim, M. Liu, and Z. L. Wang, Fiber Supercapacitors Made of Nanowire-Fiber Hybrid Structures for Wearable/Flexible Energy Storage, Angew. Chem. Int. Ed. 50 (2011) 1683-1687.
31. A. Burke, Ultracapacitors: why, how, and where is the technology, Journal of Power Sources, 91 (2000) 37-50.
32. M. Selvakumar, D. Krishna Bhat, A. Manish Aggarwal, S. Prahladh Iyer, G. Sravani, Nano ZnO-activated carbon composite electrodes for supercapacitors, Physica B, 405 (2010) 2286-2289.

33. T. Prasankumar, V. S. Irthaza Aazem, P. Raghavan, K. Prem Ananth, S.Biradar, R. Ilangovan and Sujin Jose, Microwave assisted synthesis of 3D network of Mn/Zn bimetallic oxide-high performance electrodes for supercapacitors, J. Alloys Comp., 695 (2017) , 2835-2843 .
34. D. Kalpana, K.S. Omkumar, S. Suresh Kumar, N.G. Renganathan, A novel high power symmetric ZnO/carbon aerogel composite electrode for electrochemical supercapacitor, Electrochimica Acta, 52 (2006) 1309-1315.
35. Sato K, Katayama-Yoshida H. Stabilization of ferromagnetic states by electron doping in Fe-, Co- or Ni-doped ZnO. Jpn J Appl Phys., 40 (2001) 334-340.
36. C. Cheng, G. Xu, H. Zhang, Y. Luo., Hydrothermal synthesis Ni-doped ZnO nanorods with room-temperature ferromagnetism. Mater Lett., 62 (2008) 1617-1620.
37. M.El-Hilo, A.A. Dakhel, A.Y. Ali-Mohamed, Room temperature ferromagnetism in nanocrystalline Ni-doped ZnO synthesized by co-precipitation, J Magn Magn Mater, 321 (2009) 2279-2283.
38. X. Xu, C. Cao, Hydrothermal synthesis and magneto-optical properties of Ni-doped ZnO hexagonal columns, J Magn Magn Mater, 377 (2015) 308-313.
39. M. U. Ibezim-Ezeani, F. A. Okoye, O. Akaranta, Kinetic studiem on the removal of some metal ions from aqueous solution using modified Orange mesocarp extract, Int. J. Water Res. Environ. Eng., 4 (2012) 192-200.
40. P. Amornpitoksuk , S. Suwanboon, S. Sangkanu, A. Sukhoom, N. Muensit, J. Baltrusaitis, Synthesis, characterization, photocatalytic and antibacterial activities of Ag-doped ZnOpowders modified with a diblock copolymer, Powder Technol., 219 (2012) 158-164.
41. Y. Caglar, S. Aksoy, S. Ilican, M. Caglar, Crystalline structure and morphological properties of undoped and Sn doped ZnO thin films, Superlattices Microstruct., 46 (2009) 469-475.
42. J. Cui, D. Wang, T. Xie, Y. Lin., Study on photoelectric gas-sensing property and photogenerated carrier behavior of Ag-ZnO at the room temperature, Sens Actuators B Chem.., 186 (2013) 165-171.
43. T. Sahoo, M. Kim, J. H. Baek, S. R. Jeon, J. S. Kim, Y. T. Yu, C. R. Lee, I. H. Lee, Synthesis and characterization of porous ZnO nanoparticles by hydrothermal treatment of as pure aqueous precursor, Mater Research Bull., 46 (2011) 525-530.
44. A. Escobedo Morales, M. Herrera Zaldivar, U. Pal., Indium doping in nanostructured ZnO through low-temperature hydrothermal process, Optical Materials, 29 (2006) 100-104.
45. K. Prabakar, S. Venkatachalam, Y.L. Jeyachandran, S.K. Narayandass, D. Mangalaraj., Microstructure, Raman and optical studies on Cd 0.6 Zn 0.4 Te thin films, Mater. Sci. Eng. B., 107 (2004) 99-105.
46. S. K. Mishra, S. Bayan, R. Shankar, P. Chakraborty, R. K. Srivastava., Efficient UV photosensitive and photoluminescence properties of sol–gel derived Sn doped ZnO nanostructures, Sensor Actuat A-Phys., 211 (2014) 8-14.
47. M. Ahmad, J. Zhao, J. Iqbal, W. Miao, L. Xie, R. Mo, J. Zhu, Conductivity enhancement by slight indium doping in ZnO nanowires for optoelectronic applicationsJ. Phys. D: Appl. Phys., 42 (2009) 165406-165413.
48. S.W. Xue, X.T. Zu, L.X. Shao, Z.L. Yuan, W.G. Zheng, X.D. Jiang, H. Deng, Effects of annealing on optical properties of Zn-implanted ZnO thin films, J. Alloys Compd., 458 (2008) 569-573.
49. K. Vanheusden, W.L. Warren, C.H. Seager, D.R. Tallant, J.A. Voigt, B.E. Gnade, Mechanisms behind green photoluminescence in ZnO phosphor powders, J.Appl. Phys., 79 (1996) 7983-7990.
50. G. Xiong, U. Pal, J.G. Serrano, Correlations among size, defects, and photoluminescence in ZnO nanoparticles, J. Appl. Phys., 101 (2007) 024317-024323.
51. U. Pal, P. Santiago, Controlling the morphology of ZnO nanostructures in a low-temperature hydrothermal process, J. Phys. Chem. B, 109 (2005) 15317-15321.
52. M. Liu, A.H. Kitai, P. Mascher, Point defects and luminescence centres in zinc oxide and zinc oxide doped with manganese, J. Lumin., 54 (1992) 35-42.
53. I. Shalish, H. Temkin, V.Narayanamurti, Size-dependent surface luminescence in ZnO nanowires. Phys. Rev., 69 (2004) 1-4.

54. W. E. Mahmoud, Synthesis and optical properties of Ce-doped ZnO hexagonal nanoplatelets, J. Cryst. Growth, 312 (2010) 3075–3079.
55. R. Georgekutty, M. K. Seery and S. C. Pillai, A highly efficient Ag-ZnO photocatalyst: synthesis, properties, and mechanism, J. Phys. Chem. C, 112 (2008) 13563-13570.
56. M. Arshad, A. Azam, A. S. Ahmed, S. Mollah, A. H. Naqvi, Effect of Co substitution on the structural and optical properties of ZnO nanoparticles synthesized by sol–gel route, J. Alloys Comp., 509 (2011) 8378–8381.
57. X. Sui, Y. Liu, C. Shao, Y. Liu, C. Xu, Structural and photoluminescent properties of ZnO hexagonal nanoprisms synthesized by microemulsion with polyvinyl pyrrolidone served as surfactant and passivant, Chem. Phys. Lett., 424 (2006) 340–344.
58. C. P. Sibu, S. R. Kumar, P. Mukundan, K. G. K. Warrier, Structural modifications and associated properties of lanthanum oxide doped sol-gel nanosized titanium oxide, Chem. Mater., 14 (2002) 2876-2881.
59. K. Ravichandrika, P. kiranmayi, R. V. S. S. N. Ravikumar, Synthesis,characterization and antibacterial activity of ZnO nanoparticles, Int J Pharm Pharm Sci, 4 (2012) 336-338.
60. U. Ozgür, Y. I. Alivov, C. Liu, A. Teke, M.A. Reshchikov, S. Dogan, V. Avrutin, S.J. Cho, H. Morkoc, A comprehensive review of ZnO materials and devices, J. Appl. Phys., 98 (2005) 041301-041404.
61. R. Saravanan, Kalavathy Santhi, N. Sivakumar, V. Narayanan, A. Stephen, Synthesis and characterization of ZnO and Ni doped ZnO nanorods by thermal decomposition method for spintronics application, Mater. Charact., 67 (2012) 10-16.
62. C.K. Ghosh, S. Malkhandi, M.K. Mitra, K.K. Chattopadhyay. Effect of Ni doping on the dielectric constant of ZnO and its frequency dependent exchange interaction, J Phys D: Appl Phys., 41 (2008) 245113-245119.
63. T.C.Damen, S.P.S.Porto, B.Tell, Raman effect in zinc oxide, Phys.Rev., 142 (1966) 570-574.
64. R.S. Zeferino, M.B. Flores, U. Pal, J. Appl. Phys., Photoluminescence and Raman Scattering in Ag-doped ZnO Nanoparticles, 109 (2011) 14308-14314.
65. J.M. Calleja, M. Cardona, Resonant Raman scattering in ZnO, Phys. Rev. B., 16 (1977) 3753-3761.
66. B. Yang, A. Kumar, N. Upia, P. Feng and R.S. Katiyar, Low-temperature synthesis and Raman scattering of Mn-doped ZnO nanopowders, J. Raman Spectrocs., 41 (2010) 88-92.